Hierarchical MnMoO$_4$/CoMoO$_4$ heterostructured nanowires with enhanced supercapacitor performance

Li-Qiang Mai[1,2], Fan Yang[1], Yun-Long Zhao[1], Xu Xu[1], Lin Xu[1,2] & Yan-Zhu Luo[1]

Recent attention has been focused on the synthesis and application of complex heterostructured nanomaterials, which can have superior electrochemical performance than single-structured materials. Here we synthesize the three-dimensional (3D) multicomponent oxide, MnMoO$_4$/CoMoO$_4$. Hierarchical heterostructures are successfully prepared on the backbone material MnMoO$_4$ by a simple refluxing method under mild conditions; and surface modification is achieved. We fabricate asymmetric supercapacitors based on hierarchical MnMoO$_4$/CoMoO$_4$ heterostructured nanowires, which show a specific capacitance of 187.1 F g^{-1} at a current density of 1 A g^{-1}, and good reversibility with a cycling efficiency of 98% after 1,000 cycles. These results further demonstrate that constructing 3D hierarchical heterostructures can improve electrochemical properties. 'Oriented attachment' and 'self-assembly' crystal growth mechanisms are proposed to explain the formation of the heterostructures.

---

[1] State Key Laboratory of Advanced Technology for Materials Synthesis and Processing, WUT-Harvard Joint Nano Key Laboratory, Wuhan University of Technology, Wuhan 430070, China. [2] Department of Chemistry and Chemical Biology, Harvard University, Cambridge, Massachusetts 02138, USA. Correspondence and requests for materials should be addressed to L.-Q.M. (email: mlq@cmliris.harvard.edu).

As energy storage devices with properties intermediate to those of batteries and electrostatic capacitors, electrochemical supercapacitors exhibit the desirable properties of high power density (ten times more than batteries), fast charging (with seconds), excellent cycling stability, small size and low mass, which make them one of the most promising candidates for next-generation power devices[1–7]. With characteristics complementary to those of rechargeable batteries and fuel cells, supercapacitors have been used in many applications, such as power back-up, pacemakers, air bags and electrical vehicles[8]. Currently, most commercial supercapacitors are made of high-surface-area carbonaceous materials[2]. However, these supercapacitors might not provide sufficient energy/power densities or efficiencies, and the specific capacitance severely decreases under high current. Therefore, much attention has been focused on improving the capacitance of supercapacitors, and their performance at high current densities, by constructing complex heterostructures with increased surface areas.

Three-dimensional (3D) hierarchical heterostructures with high surface/body ratios, large surface areas, better permeabilities and more surface active sites have potential in optical, catalytic and electrochemical applications[9–15]. Thus, the synthesis and application of 3D hierarchical heterostructures will be a focus of the nanomaterial research field[16–19]. Mai et al. have synthesized ultra-long hierarchical vanadium oxide nanowires by electrospinning, which exhibit much higher capacity in lithium ion batteries[20]. Meng et al. synthesized 3D Bi_2WO_6/TiO_2 to enhance photocatalytic activity and found that the heterostructures exhibited much higher photodegradation efficiency than Bi_2WO_6 and TiO_2 (ref. 19).

The molybdates $MnMoO_4$ and $CoMoO_4$ have excellent catalytic and electrochemical characteristics[21–23]. In this paper, hierarchical $MnMoO_4/CoMoO_4$ heterostructured nanowires were controllably synthesized using a facile refluxing method under mild conditions. $MnMoO_4$ nanowires form the backbone material, and the $CoMoO_4$ shell thickness could be tuned by changing the molar ratio of Mn source and Co source. The superior electrochemical performance of the structure was demonstrated.

Results

Characterization of $MnMoO_4/CoMoO_4$ heterostructured nanowires. To determine the phase structures of the products, the X-ray diffraction (XRD) measurements were conducted. The backbone material $MnMoO_4$ nanowires ($MnMoO_4$: JCPDS card No. 01-072-0285; $MnMoO_4 \cdot 0.9H_2O$: JCPDS card No. 00-050-1286) were identified by the XRD pattern shown in Figure 1a (black line). The hierarchical $MnMoO_4/CoMoO_4$ heterostructured nanowires (open circles, open squares: JCPDS card No.00-021-0868) were identified in Figure 1a (red line). Because $MnMoO_4$ (No.01-084-2102: $a = 10.469$ Å, $b = 9.516$ Å, $c = 7.143$ Å) has a similar crystal lattice parameter as $CoMoO_4$ (No.00-021-0868: $a = 10.210$ Å, $b = 9.268$ Å, $c = 7.022$ Å), lattice matching between $MnMoO_4$ and $CoMoO_4$ can exist. Raman

spectroscopy was applied to further investigate the structural change in bonding related to the hierarchical heterostructure (Fig. 1b). For those structures, the strong bands observed between 200 and 1,200 cm^{-1} can be assigned to bend and stretching frequencies of those materials. The band at 872 cm^{-1} in hierarchical $MnMoO_4/CoMoO_4$ heterostructured nanowires was not found in pure $CoMoO_4$ nanorods or backbone $MnMoO_4$ nanowires, which may be assigned to the new stretching vibration of Co–O–Mn.

Figure 2a–d shows the scanning electron microscopy (SEM) images of the $MnMoO_4$ nanowires and obtained $MnMoO_4/CoMoO_4$ heterostructured nanowires. In Figure 2a, pure $MnMoO_4$ nanowires with the length of 10 μm and the diameter of 500 nm were used as the backbone material. The hierarchical heterostructures of the $MnMoO_4/CoMoO_4$ sample are shown in Figure 2b–e. With the extension of reaction time, $CoMoO_4$ nanorods with higher density grew aslant on the primary $MnMoO_4$ nanowires (Supplementary Fig. S1). Further information about $MnMoO_4/CoMoO_4$ hierarchical heterostructure was obtained from transmission electron microscopy (TEM) (Fig. 2d). It is confirmed that $CoMoO_4$ nanorods have diameters of about 50 nm. Close inspection at the heterojunction shows that the $CoMoO_4$ nanorods have their roots inside the $MnMoO_4$ nanowires, suggesting that the $CoMoO_4$ nanorods are not just loosely attached to the nanowire surface. The high-resolution TEM investigation (Fig. 2e) demonstrates that the interlayer distances are consistent with the interplanar distances of $CoMoO_4$ (0.335 nm) and $MnMoO_4$ (0.288 nm). These results suggest that the prepared sample is considered to be a well-crystallized heterostructure with $MnMoO_4/CoMoO_4$ on nanoscale. Energy dispersive spectroscopy (EDS) microanalysis on selected areas was shown in Figure 2f. The 'shell' of the heterostructures consists of Co, Mo and O (the inset of Fig. 2f) elements, whereas the entire heterostructures consist of Mn, Co, Mo and O (Fig. 2f), indicating that the nanorods grown on the surface are mainly made of $CoMoO_4$ and the parent hierarchical heterostructures are a mixture of $MnMoO_4$ and $CoMoO_4$, which agrees well with the results of XRD analysis. A $MnMoO_4/CoMoO_4$ nanocomposite without 3D hierarchical heterostructures was also synthesized by a simple refluxing method, as a control experiment (Supplementary Fig. S2).

Crystal growth mechanism. The crystal growth mechanism of 'self-assembly' and 'oriented attachment' were proposed to demonstrate the complicated nano-architecture process. The oriented attachment mechanism describes the spontaneous self-organization of adjacent particles, so that they share a common crystallographic orientation, followed by the joining of these particles at a planar interface. The process is particularly relevant in the nanocrystalline regime, where bonding between the particles reduces overall energy by removing surface energy associated with unsatisfied bonds[24]. In the reaction, $MnMoO_4$ nanowires were used as the 'substrate', which can guide the $CoMoO_4$ self-assembling growth in aqueous solution without surfactant and stabilizers. Then the 'oriented attachment' can guide the nanoparticles oriented growth. As shown in Figure 3, supersaturated solution with plenty of $CoMoO_4$ small crystals were formed by adding Co resource. Because of the high surface energy and thermodynamics instability, nanoparticles can attach to the surface of $MnMoO_4$ to decrease surface energy. The crystallographic orientation of the particles with respect to each other is determined by the minimization of the highest surface energy. Therefore, with a matching lattice, the lattice fringes' orientation and crystal growth direction are uniform to some extent. The 'substrate', $MnMoO_4$, has similar lattice parameters and can control $CoMoO_4$ nanoparticle self-assembly and oriented crystallization to form hierarchical $MnMoO_4/CoMoO_4$ heterostructured nanowires.

Electrochemical properties. Figure 4a,b displays the galvanostatic charge–discharge curves of hierarchical $MnMoO_4/CoMoO_4$
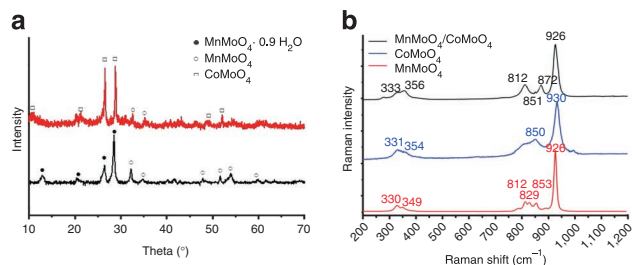
Figure 1 | Phase analysis. (a) XRD patterns of backbone $MnMoO_4$ nanowires (black line) and hierarchical $MnMoO_4/CoMoO_4$ heterostructured nanowires (red line). **(b)** Raman spectra of hierarchical $MnMoO_4/CoMoO_4$ heterostructured nanowires, pure $CoMoO_4$ nanorods and backbone $MnMoO_4$ nanowires.
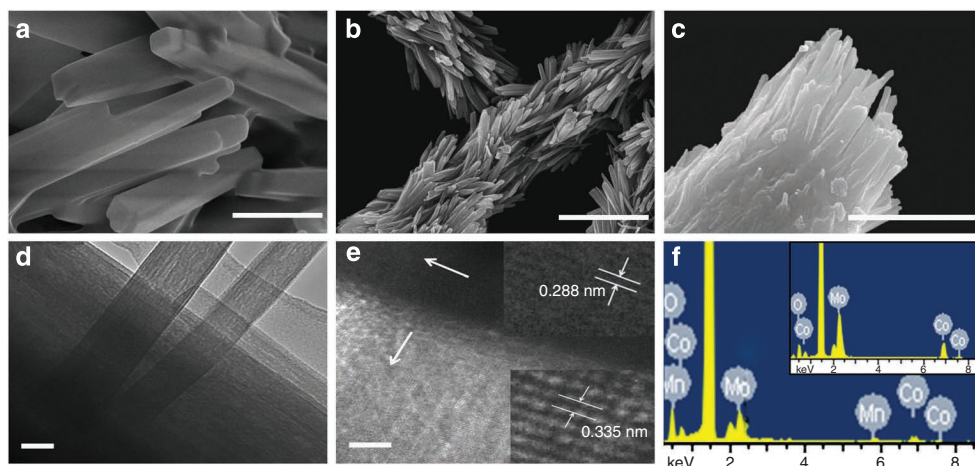
Figure 2 | Morphology characterization. (**a**) SEM image of the backbone MnMoO$_4$ nanowires. (**b**, **c**) SEM images of hierarchical MnMoO$_4$/CoMoO$_4$ heterostructured nanowires. (**d**, **e**) TEM and high-resolution TEM images at the heterojunction of hierarchical MnMoO$_4$/CoMoO$_4$ heterostructured nanowires. (**f**) The EDS microanalysis on selected areas. Scale bars, 1 µm (**a**–**c**); 20 nm (**d**); 5 nm (**e**).
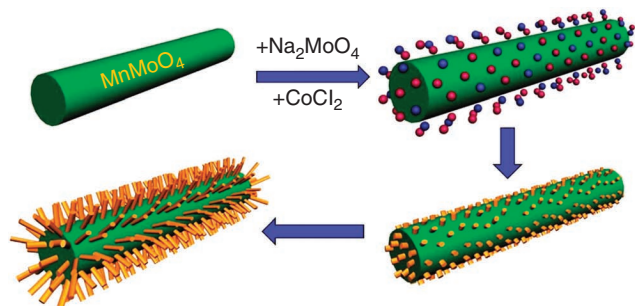
Figure 3 | The construction of hierarchical MnMoO$_4$/CoMoO$_4$ nanowires. The green rod represents the backbone MnMoO$_4$ nanowire, and orange rods the CoMoO$_4$ nanorods. Red and blue balls are different ions dispersed in the aqueous solution.

heterostructured nanowires and MnMoO$_4$/CoMoO$_4$ nanocomposite (No 3D), MnMoO$_4$ nanowires, CoMoO$_4$ in 2 M NaOH at room temperature. The specific capacitance has been calculated from equation (1):

$$C(F/g) = \frac{i\Delta t}{m\Delta V} \quad (1)$$

Where i (A) is the current density used for charge/discharge, Δt(s) is the time elapsed for the discharge cycle, m (g) is the weight of the active electrode and ΔV (V) is the voltage interval of the discharge. The specific capacitance and energy density calculated from each discharge curve are shown in Figure 4c. The hierarchical MnMoO$_4$/CoMoO$_4$ electrodes can reach to 204.1, 187.1, 163.4, 134.7 F g^{-1} and 28.4, 26.0, 22.7, 18.7 Wh kg^{-1} at 0.5, 1, 2, 3 A g^{-1}. The capacitance for hierarchical MnMoO$_4$/CoMoO$_4$ heterostructured nanowires is significantly higher than that for pure one-dimensional nanorods (MnMoO$_4$: 9.7 F g^{-1}, 8.8 Wh kg^{-1}; CoMoO$_4$: 62.8 F g^{-1}, 1.4 Wh kg^{-1}; MnMoO$_4$/CoMoO$_4$ nanocomposite: 69.2 F g^{-1}, 9.6 Wh kg^{-1} at a charge–discharge current density of 1 A g^{-1}). The hierarchical MnMoO$_4$/CoMoO$_4$ heterostructured nanowire electrode exhibited good reversibility with cycling efficiency of 98% after 1,000 cycles shown in Figure 4d.
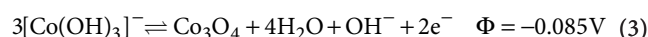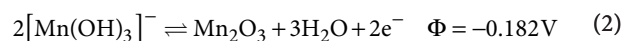
As reported, at low current densities, due to the low ohmic drop, the inner active sites or the pores of the electrode can be fully accessed; hence, high specific capacitance values can be achieved[25]. However, high current densities are of great importance in industrial applications. The measuring conditions of hierarchical MnMoO$_4$/CoMoO$_4$ heterostructured nanowires were implemented at higher current
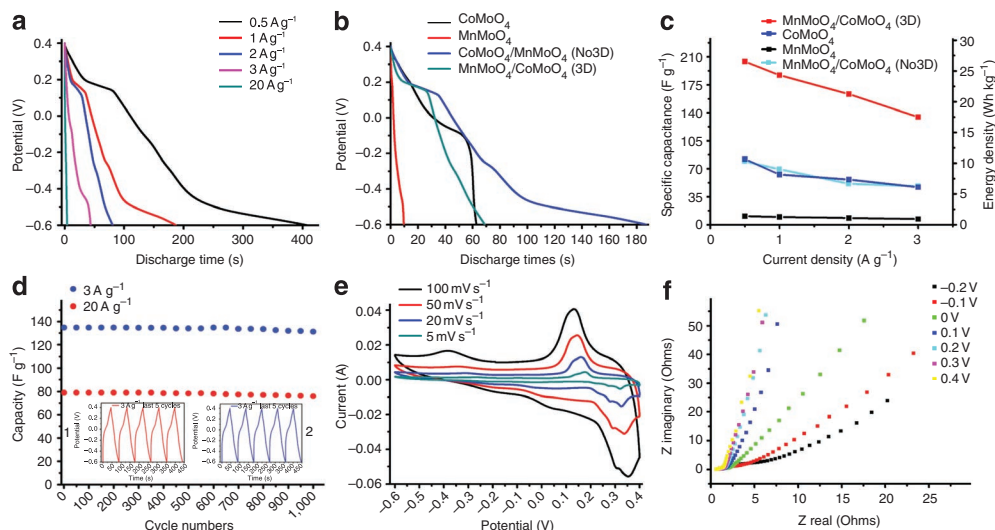
densities. The result reveals that the observed specific capacitance values 204.1 F g^{-1} for the hierarchical MnMoO$_4$/CoMoO$_4$ electrodes are higher than those reported, such as MoO$_2$ (ref. 3), MnO$_2$ (ref. 26) and Co$_3$O$_4$ (ref. 27), at similar current densities to a certain extent.
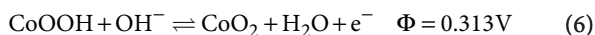
Discussion

To explain the electrochemical results, it is important to consider the hierarchical MnMoO$_4$/CoMoO$_4$ heterostructured nanowires that exert such a significant influence on charge storage. This consideration is closely related to the Brunauer–Emmet–Teller (BET) surface area (Supplementary Fig. S3). The BET surface area of MnMoO$_4$ is 3.17 m^2 g^{-1}, MnMoO$_4$/CoMoO$_4$ nanocomposite is 28.0 m^2 g^{-1} and MnMoO$_4$/CoMoO$_4$ (3D) after surface modification can reach to 54.06 m^2 g^{-1}, which is larger than that reported in the literature (MnMoO$_4$ nanorods 15 m^2 g^{-1} and CoMoO$_4$ nanorods 25 m^2 g^{-1} with smaller size[28]), so the inner active sites of the electrode can be fully accessed with large surface area. Besides, compared with self-aggregated short CoMoO$_4$ and MnMoO$_4$ nanorods synthesized by hydrothermal and micro-emulsion method, the hierarchical MnMoO$_4$/CoMoO$_4$ heterostructured nanowires exhibit much higher capacity. This is due to the fact that self-aggregation of the hierarchical MnMoO$_4$/CoMoO$_4$ heterostructured nanowires have been greatly reduced, which can keep the effective contact areas of active materials and electrolyte large and sufficient. Third, in comparison with pure CoMoO$_4$ nanorods, the highly dense small CoMoO$_4$ nanorods grow on the MnMoO$_4$ 'substrate' orderly but with low crystallinity. This structure can provide surface sites for redox reaction, and possess sufficient order to enable OH$^-$ access to the heterostructures facilely. It would seem, therefore, that the facile ability of OH$^-$ to be inserted is an extra account for the enhanced charge storage of hierarchical MnMoO$_4$/CoMoO$_4$ heterostructured nanowires. These factors are expected to contribute to the substantial level of capacitive ability for supercapacitors.

The cyclic voltammogram (CV) is performed to identify the charge storage mechanism in MnMoO$_4$/CoMoO$_4$. Figure 4e shows the CVs of MnMoO$_4$/CoMoO$_4$. Comparing to the MnMoO$_4$ and CoMoO$_4$ electrodes (Supplementary Fig. S4), one more pair of redox peaks can be observed in the CV curves of MnMoO$_4$/CoMoO$_4$, which can indicate that the pseudocapacitance mainly comes from the Faradic redox reaction of both Mn and Co. Comparing to the Pourbaix diagram of Mn, Co and Mo (Supplementary Fig. S5)[29], Faradic redox reactions are as follows:

$$2[Mn(OH)_3]^- \rightleftharpoons Mn_2O_3 + 3H_2O + 2e^- \quad \Phi = -0.182\,V \quad (2)$$

$$3[Co(OH)_3]^- \rightleftharpoons Co_3O_4 + 4H_2O + OH^- + 2e^- \quad \Phi = -0.085\,V \quad (3)$$

Figure 4 | Electrochemical characterizations in 2 M NaOH aqueous solution at room temperature. (**a**) Galvanostatic charge–discharge curves of hierarchical $MnMoO_4/CoMoO_4$ heterostructured nanowire electrodes at different current density. (**b**) Galvanostatic charge–discharge curves of $MnMoO_4$, $CoMoO_4$, $MnMoO_4/CoMoO_4$ nanocomposite (No 3D), $MnMoO_4/CoMoO_4$ (3D) electrodes at current density of $1\,g^{-1}$. (**c**) Specific capacitance and energy density of different electrodes at different current density. (**d**) Charge–discharge cycling test of $MnMoO_4/CoMoO_4$ (3D) electrodes at the current density of 3 and $20\,A\,g^{-1}$, showing 2% loss after 1,000 cycles; inset shows the galvanostatic charge–discharge cyclic curves of the first and last five cycles at $3\,A\,g^{-1}$. (**e**) Cyclic voltammogram curves of $MnMoO_4/CoMoO_4$ (3D) electrodes. (**f**) AC impedance plots of $MnMoO_4/CoMoO_4$ electrodes.

$$Co_3O_4 + H_2O + OH^- \rightleftharpoons 3CoOOH + e^- \quad \Phi = 0.036\,V \quad (4)$$

$$Mn_2O_3 + 2OH^- \rightleftharpoons 2MnO_2 + H_2O + 2e^- \quad \Phi = 0.306\,V \quad (5)$$

$$CoOOH + OH^- \rightleftharpoons CoO_2 + H_2O + e^- \quad \Phi = 0.313\,V \quad (6)$$

Supplementary Figure S4 and Figure 4e show that with the increase of the scan rate, the redox current increased, the anodic peak shifted towards positive potential and the cathodic peak shifted towards negative potential. The peak current increases nearly linearly with the scan rate confirming the pseudocapacitive behaviour. The increase of the current response with the scan rate also indicates that the kinetics of interfacial Faradic redox reactions and the rates of electronic and ionic transport are even rapid enough at scan rates as high as $100\,mV\,s^{-1}$.

Figure 4f displays the Nyquist plots of $MnMoO_4/CoMoO_4$ at different voltage. The semicircle in the high-frequency range corresponds to the charge-transfer resistance caused by the Faradic reaction, which was correlated with the intercalation and deintercalation of cations. Between 0.1–0.4 V, the plots in the low-frequency range correspond to the diffusion-limited mechanism, which confirms that the main pseudocapacitive behaviour occurred between 0.1–0.4 V. The result is concordant with the two pairs of redox peaks of CVs.

In summary, a mild facile refluxing method was used to fabricate hierarchical $MnMoO_4/CoMoO_4$ heterostructured nanowires possessing a specific capacitance of $187.1\,F\,g^{-1}$ at a high current density of $1\,A\,g^{-1}$ and a good reversibility with cycling efficiency of 98% after 1,000 cycles. This demonstrates that constructing hierarchical $MnMoO_4/CoMoO_4$ nanowire heterostructures by combining 'oriented attachment' and 'self-assembly' is a significant and simple route to improve electrochemical properties. The hierarchical $MnMoO_4/CoMoO_4$ nanowire heterostructure described in this paper may have potential applications in energy storage and other electrochemical devices.

Methods

Synthesis of $MnMoO_4/CoMoO_4$ heterostructured nanowires. $MnMoO_4$ nanowires, the backbone material, were prepared by simple micro-emulsion method with Na_2MoO_4 and $MnCl_2$. The synthesis of hierarchical $MnMoO_4/CoMoO_4$ heterostructured nanowires was performed in a flask with mild magnetic

stirring for different periods. Typically, $MnMoO_4$ nanowires were dispersed in 40 ml water and the dispersion was refluxed at 60 °C. Then, $CoCl_2$ and the same amount of Na_2MoO_4 were added to the mother solution discontinuously. To follow the crystal growth process, the samples were taken at different time intervals. Then the sample was washed with deionized water and ethanol, and dried for further characterization. The $CoMoO_4$ shell thickness could be tuned by changing the molar ratio of Mn source and Co source.

Characterization and electrochemical measurement. The crystal phase and purity of the product were characterized by X-ray powder diffraction. XRD patterns of the products were recorded on a Rigaku D/MAX-III diffractometer (Rigaku) with monochromatized Cu Ka radiation ($k = 1.5406\,\text{Å}$). SEM performed on JSM-5610LV was used to characterize the morphology of the synthesized nanomaterials. TEM, high-resolution TEM were recorded by using a JEOL JEM-2010 FEF microscope (JEOL) at an accelerating voltage of 200 kV. EDS was performed on a JEM 2100F STEM/EDS and the X-ray energy resolution is 132 eV. Laser Raman spectrometer was recorded using the INVIA, Renishaw. BET surface areas were measured using Gemini 2360 instrument by adsorption of nitrogen at −209 °C. A three electrodes method consisting of an nickel foam as working electrode (0.07 cm²), Pt wire and Ag/AgCl (saturated KCl) electrodes as counter and reference electrodes were used. Cyclic voltammetry and galvanostatic charge–discharge studies were performed using an Autolab Potentiostat Galvanostat. NaOH (2.0 M) was used as the electrolyte. The working electrode consisted of 60 wt% of the active material (for example, $MnMoO_4/CoMoO_4$), 35.5 wt% of conductivity agent (carbon black, Super-P-Li) and 4.5 wt% of binder (polytetrafluoroethylene).

References

1. Miller, J. R., Outlaw, R. A. & Holloway, B. C. Graphene double-layer capacitor with ac line-filtering performance. *Science* **329,** 1637–1639 (2010).
2. Chen, P. C., Shen, G. Z., Shi, Y., Chen, H. T. & Zhou, C. W. Preparation and characterization of flexible asymmetric supercapacitors based on transition-metal-oxide nanowire/single-walled carbon nanotube hybrid thin-film electrodes. *ACS Nano* **4,** 4403–4411 (2010).
3. Rajeswari, J., Kishore, P. S., Viswanathan, B. & Varadarajan, T. K. One-dimensional MoO_2 nanorods for supercapacitor applications. *Electrochem. Commun.* **11,** 572–575 (2009).
4. Pech, D. *et al.* Ultrahigh-power micrometre-sized supercapacitors based on onion-like carbon. *Nat. Nanotechnol.* **5,** 651–654 (2010).
5. Conway, B. E. *Electrochemical Supercapacitors-Scientic Fundamentals and Technological Applications* (KluwerAcademic/Plenum Publishers, 1999).
6. Lee, S. W. *et al.* High-power lithium batteries from functionalized carbon-nanotube electrodes. *Nat. Nanotechnol.* **5,** 531–537 (2010).
7. Brezesinski, T., Wang, J., Tolbert, S. H. & Dunn, B. Ordered mesoporous α-MoO_3 with iso-oriented nanocrystalline walls for thin-film pseudocapacitors. *Nat. Mater.* **9,** 146–151 (2010).

8. Miller, J. R. & Simon, P. Materials science—electrochemical capacitors for energy management. *Science* **321,** 651–652 (2008).
9. Li, J. F. *et al.* Shell-isolated nanoparticle-enhanced Raman spectroscopy. *Nature* **464,** 392–395 (2010).
10. Bae, J. *et al.* Fiber supercapacitors made of nanowire-fiber hybrid structures for wearable/flexible energy storage. *Angew. Chem. Int. Ed.* **50,** 1683–1687 (2011).
11. Dong, Y. J., Yu, G. H., McAlpine, M. C., Lu, W. & Lieber, C. M. Si/a-Si core/shell nanowires as nonvolatile crossbar switches. *Nano Lett.* **8,** 386–391 (2008).
12. Myung, Y. *et al.* Composition-tuned ZnO-CdSSe core-shell nanowire arrays. *ACS Nano* **4,** 3789–3800 (2010).
13. Sun, Y. K. *et al.* High-energy cathode material for long-life and safe lithium batteries. *Nat. Mater.* **8,** 320–324 (2009).
14. Liang, W. J., Yuhas, B. D. & Yang, P. D. Magnetotransport in Co-doped ZnO nanowires. *Nano Lett.* **9,** 892–896 (2009).
15. Zhang, Q., Chen, X. Y., Zhou, Y. X., Zhang, G. B. & Yu, S. H. Synthesis of $ZnWO_4$@MWO_4 (M=Mn, Fe) core-shell nanorods with optical and antiferromagnetic property by oriented attachment mechanism. *J. Phys. Chem. C* **111,** 3927–3933 (2007).
16. Tao, A. R., Ceperley, D. P., Sinsermsuksakul, P., Neureuther, A. R. & Yang, P. D. Self-organized silver nanoparticles for three-dimensional plasmonic crystals. *Nano Lett.* **8,** 4033–4038 (2008).
17. Niu, M. T. *et al.* Hydrothermal synthesis, structural characteristics, and enhanced photocatalysis of SnO_2/alpha-Fe_2O_3 semiconductor nanoheterostructures. *ACS Nano* **4,** 681–688 (2010).
18. Chen, F. *et al.* Large-scale and shape-controlled syntheses of three-dimensional CdS nanocrystals with flowerlike structure. *J. Phys. Chem. C* **112,** 1001–1007 (2008).
19. Shang, M. *et al.* 3D Bi_2WO_6/TiO_2 hierarchical heterostructure: Controllable synthesis and enhanced visible photocatalytic degradation performances. *J. Phys. Chem. C* **113,** 14727–14731 (2009).
20. Mai, L. Q. *et al.* Electrospun ultralong hierarchical vanadium oxide nanowires with high performance for lithium ion batteries. *Nano Lett.* **10,** 4750–4755 (2010).
21. Kim, S. S., Ogura, S., Ikuta, H., Uchimoto, Y. & Wakihara, M. Reaction mechanisms of $MnMoO_4$ for high capacity anode material of Li secondary battery. *Solid State Ionics* **146,** 249–256 (2002).
22. Ehrenberg, H., Schwarz, B. & Weitzel, H. Magnetic phase diagrams of alpha-$MnMoO_4$. *J. Magn. Magn. Mater.* **305,** 57–62 (2006).
23. Singh, R. N., Singh, J. P. & Singh, A. Electrocatalytic properties of new spinel-type $MMoO_4$ (M=Fe, Co and Ni) electrodes for oxygen evolution in alkaline solutions. *Int. J. Hydrogen Energ.* **33,** 4260–4264 (2008).
24. Niederberger, M. & Colfen, H. Oriented attachment and mesocrystals: non-classical crystallization mechanisms based on nanoparticle assembly. *Phys. Chem. Chem. Phys.* **8,** 3271–3287 (2006).
25. Morishita, T., Soneda, Y., Hatori, H. & Inagaki, M. Carbon-coated tungsten and molybdenum carbides for electrode of electrochemical capacitor. *Electrochim. Acta* **52,** 2478–2484 (2007).
26. Nakayama, M., Tanaka, A., Sato, Y., Tonosaki, T. & Ogura, K. Electrodeposition of manganese and molybdenum mixed oxide thin films and their charge storage properties. *Langmuir* **21,** 5907–5913 (2005).
27. Shinde, V. R., Mahadik, S. B., Gujar, T. P. & Lokhande, C. D. Supercapacitive cobalt oxide (Co_3O_4) thin films by spray pyrolysis. *Appl. Surf. Sci.* **252,** 7487–7492 (2006).
28. Ding, Y., Wan, Y., Min, Y. L., Zhang, W. & Yu, S. H. General synthesis and phase control of metal molybdate hydrates $MMoO_4 \cdot nH_2O$ (M=Co, Ni, Mn, n=0, 3/4, 1) nano/microcrystals by a hydrothermal approach: magnetic, photocatalytic, and electrochemical properties. *Inorg. Chem.* **47,** 7813–7823 (2008).
29. Takeno, N. Atlas of Eh-pH diagrams Intercomparison of thermodynamic databases. *National Institute of Advanced Industrial Science and Technology* (2005).

Acknowledgements

Author contributions

Y.-L.Z. and F.Y. performed the experiments. L.-Q.M., Y.-L.Z. and F.Y. designed the experiments, discussed the interpretation of results and co-wrote the paper. All authors discussed the results and commented on the manuscript.

Additional information

Supplementary Information accompanies this paper at http://www.nature.com/naturecommunications

Competing financial interests: The authors declare no competing financial interests.

Reprints and permission information is available online at http://npg.nature.com/reprintsandpermissions/

How to cite this article: Mai, L.-Q. *et al.* Hierarchical $MnMoO_4$/$CoMoO_4$ heterostructured nanowires with enhanced supercapacitor performance. *Nat. Commun.* 2:381 doi: 10.1038/ncomms1387 (2011).